Preparation, crystal structures, experimental and theoretical electronic band structures of cobalt tellurides in the composition range $CoTe_{1.3}$-$CoTe_2$

1998 J. Phys.: Condens. Matter 10 2947

(http://iopscience.iop.org/0953-8984/10/13/012)

J. Phys.: Condens. Matter **10** (1998) 2947–2962. Printed in the UK PII: S0953-8984(98)88713-4

Preparation, crystal structures, experimental and theoretical electronic band structures of cobalt tellurides in the composition range $CoTe_{1.3}$–$CoTe_2$

M Muhler†, W Bensch‡§ and M Schur‡

† Institut für Technische Chemie, Ruhr-Universität Bochum, D-44780 Bochum, Germany
‡ Institut für Anorganische Chemie, Christian-Albrechts-Universität Kiel, Olshausenstrasse 40, D-24098 Kiel, Germany

Received 27 October 1997

Abstract. Cobalt tellurides in the composition range $CoTe_{1.3}$–$CoTe_2$ crystallize in a CdI_2-type structure with short intra- and interslab Te–Te contacts indicating a polymeric network with multiple Te–Te bonds explaining the very low c/a values of 1.38 to 1.41 of the hexagonal cells. Single-crystal x-ray investigations performed on $CoTe_2$ confirm the marcasite-type structure in the centrosymmetric space group $Pnnm$.

Experimental valence band spectra (UPS) confirm that the Co tellurides in the composition range $CoTe_x$ ($1.3 < x < 2$) are metals. The emission at the Fermi level E_F decreases with the Te content and is due to Co 3d and Te 5p states. This assignment is supported by the results of the calculated density of states curve (DOS) which demonstrates that Te p states contribute about 50% in the CdI_2-type and about 35% in the marcasite-type structure. The Te d states contribute about 15% to the total Te contributions. This behaviour cannot be understood on the basis of a simple tight-binding description, ignoring d-valence states of Te.

Core level spectra (XPS) suggest that all $CoTe_x$ samples are best described as intermetallic compounds. Small chemical shifts between the different samples are mainly due to the different Madelung contributions rather than to changes of the electron density located on the Co atoms. An oxidation number for Te < -1 in all $CoTe_x$ samples is deduced, in good agreement with the value of about -1.3 for the Te in $CoTe_2$ that would be deduced from the relation between the Te–Te distances versus oxidation states of the anion in $(Te_2)^{-II}$, Te^{-II}. The three-dimensional character of the Co tellurides deduced from the crystal structure is further confirmed by the calculated energy dispersion $E(k)$.

1. Introduction

In a number of studies concerning the bonding properties in transition metal ditellurides it was demonstrated that the 'classical' description of the bonding properties of ditellurides of the late transition elements with the CdI_2-type structure corresponding to $M^{IV}(Te^{-II})_2$ does not adequately illuminate the bonding situation [1–6]. The formation of three-dimensional pyrite and marcasite structures on the right side of the periodic table reflects the destabilization of the higher oxidation states of the cations when going from the left to the right of the periodic table. This observation is in line with the successive lowered energy of the d electronic band levels, the loss of directionality of the bonds when moving from sulphur to tellurium and the decrease of electronegativity within the column, which leads to

§ Corresponding author.

0953-8984/98/132947+16$19.50

an essentially sp valence band higher in energy. The lower d levels of the elements on the right of the periodic table and the energetically higher sp valence band of tellurium may lead to a d cationic/sp anionic redox competition making further studies of the ditellurides of particular interest. In the past the Co–Te system was intensively investigated with respect to the crystallographical, thermal, electrical and magnetic properties [7–24]. In the composition range Co:Te = 1:1–1:2 only two distinct phases exist. The trigonal CdI_2 type is stable between $CoTe_{1.19}$ and $CoTe_{1.79}$ [7, 8] with very low c/a ratios ranging from 1.380 to 1.423 [7, 11, 16]. A further decrease of the Co content leads to the formation of the orthorhombic marcasite-type structure, which occurs at a composition $CoTe_{1.98}$ for samples annealed at 450 °C and is stable up to $CoTe_{2.29}$ [10–12]. In the composition range $CoTe_{1.79}$–$CoTe_{1.98}$ the CdI_2 and orthorhombic phases coexist. It was reported that $CoTe_2$ with the marcasite-type structure melts peritectically at 764 °C [11].

From the continuous variation of the magnetic susceptibility, thermal and electrical conductivity in the region of the CdI_2-type structure it was concluded that no ordered structures exist in this composition range. Magnetic measurements showed a Curie–Weiss-like behaviour with little dependency on temperature [16, 22] and a smooth decrease of susceptibility with increasing Te content [7]. The weak temperature dependence observed for some compositions is ascribed to a Pauli paramagnetism [19]. A more detailed explanation of the magnetic properties is given by [20] using a model of fluctuating magnetic moments. The CdI_2 phase as well as the marcasite-type ditelluride show metallic conductivity [12, 19] and the sign of the Seebeck coefficient as well as its temperature dependence are in agreement with the metallic behaviour [7]. The bonding properties of cobalt tellurides were studied by ^{125}Te Mössbauer spectroscopy [13, 23]. For $CoTe_2$ an effective charge of -1.61 for Te was calculated. Mössbauer studies confirmed the absence of a stochiometric CoTe phase and the presence of two different crystallographic sites according to a fully and a partly occupied Co layer respectively [21]. High absorption for the composition Co_2Te_3 led to the assumption of the existence of a superstructure. In addition a minimum of formation enthalphy for this composition was assumed by the fact that it is found in crystals grown by chemical transport reactions [15]. X-ray absorption spectroscopy performed on the Co K edge showed shifts of 0.5 eV and 1.21 eV for CoTe and $CoTe_2$ relative to metallic Co [9].

In a previous contribution concerning the bonding properties of nickel ditelluride we demonstrated that $NiTe_2$ can be viewed as a true three-dimensional compound with appreciable Te–Te bonding interactions [6]. We also demonstrated that stoichiometric $NiTe_2$ does not exist but the deviation from stoichiometry is very small [6]. As was noted in an earlier study the c/a ratios for $Ni_{1+x}Te_2$ and $CoTe_{1.7}$ are very similar and cannot be explained on the basis of the differences of the ionic radii of Ni^{n+} and Co^{n+} ($n = 2$, 3 or 4) [1]. It is also interesting to notice that $CoTe_2$ adopts the marcasite-type structure whereas $NiTe_2$ crystallizes in a polymeric CdI_2-type structure [1]. To obtain a better understanding of the bonding properties as well as of the physical properties of the late transition metal tellurides we decided to reinvestigate the Co–Te system in the composition range $CoTe_{1.3}$–$CoTe_2$. The present contribution reports the results of crystal structure determination, experimental band structure investigations using XPS and UPS and electronic band structure calculations based on the LMTO niveau.

2. Experiment

Different $CoTe_x$ samples ($x = 1.3$, 1.6, 1.7, 1.8, 1.9 and 2.0) were prepared by heating the elements in evacuated and sealed silica tubes. Prior to use the ampoules were heated in order

to remove adsorbed oxygen or H_2O. The elements were used as delivered (Heraeus AG; Co: 99.9%; Te: 99.9999%). The mixtures were heated to 870 K at 100 K h^{-1} and kept at this temperature for one week. In the case of $CoTe_2$ phase equilibrium was achieved by heating the ground sample for another 7 weeks at 720 K. The absence of the hexagonal $CoTe_x$ phase was confirmed by x-ray powder diffractometry. The products were characterized with x-ray powder diffractometry (STOE STADI P diffractometer; Cu Kα, $\lambda = 1.540\,56$ Å).

Table 1. Technical details of data acquisition and selected refinement results for $CoTe_2$ and $CoTe_{1.3}$. Note: $CoTe_{1.3}$ was twinned with a twin fraction of 27(1)%. The refinement was performed with the SHELXL 93 software.

	$CoTe_2$	$CoTe_{1.3}$
Space group	$Pnnm$	$P-3m1$
Cell parameters [Å]	$a = 5.3267(5)$	$a = 3.893(1)$
	$b = 6.3219(4)$	$c = 3.9059(3)$
	$c = 5.371(1)$	
Cell volume [Å^3]	131.53	70.49(3)
Absorption coefficient [mm^{-1}]	27.87	18.89
Extinction parameter x	0.0110(5)	0.16(2)
Measured reflections	2268	781
	$-9 \leqslant h \leqslant 9, -10 \leqslant k \leqslant 10$	$-5 \leqslant h \leqslant 5, -5 \leqslant k \leqslant 5, -7 \leqslant l \leqslant 7$
	$-6 \leqslant l \leqslant 6$	
Independent reflections	307	103
Used reflections ($F_o \geqslant nF_o$)	307 ($n = 4$)	103 ($n = 2$)
Number of variables	12	9
R/R_w [%]	1.70, 2.04	2.13, 4.04[a]
Weight $y/a, b$	0.0015	0.0106/0.185
GOF	1.47	1.356
Max. difference peaks [e Å^{-3}]	$2.12/-2.10$	$0.81/-1.70$

[a]Definition used in the SHELXTL plus software ($CoTe_2$):
weight: $w = 1/(\sigma^2(F_o) + yF^2)$
extinction correction: $F_c^* = F_c[1 + 0.002xF_c^2/\sin(2\Theta)]^{-1/4}$
Definitions used in the SHELXL 93 software ($CoTe_{1.3}$):
weight: $w = 1/[\sigma^2(F_o^2) + (aP)^2 + bP]$ where $P = (\max(F_o^2 \text{ or } 0) + 2F_c^2)/3$
extinction correction: $F_c^* = kF_c[1 + 0.001xF_c^2\lambda^3/\sin(2\Theta)]^{-1/4}$
$wR2$ used instead of R_w: $w_{R2} = [\Sigma[w(F_o^2 - F_c^2)^2]/\Sigma[w(F_o^2)^2]]^{1/2}$

For the single-crystal investigation a needle shaped crystal of $CoTe_2$ and a hexagonal platelet of $CoTe_{1.3}$ were selected. Intensity data were recorded on an STOE AED II diffractometer (graphite monochromated Mo Kα radiation, $\lambda = 0.7107$ Å) in the $\Theta/2\Theta$ scan mode. The intensities were reduced to F_o by applying Lorentz polarization corrections. Numerical absorption corrections (indexed faces) were also performed. Some technical details of the data collection as well as refinement results are summarized in table 1. Atomic coordinates, isotropic and anisotropic displacement factors are listed in table 2 and selected interatomic distances are given in table 3. All calculations for the ditelluride were undertaken with the software package SHELXTL plus using scattering factors for neutral atoms. Because the $CoTe_{1.3}$ crystal was twinned the refinement of the structure was performed with the SHELXL 93 software. Lists of structure factors are available on request from the authors. X-ray photoelectron spectroscopy (XPS, Mg Kα = 1253.6 eV) and ultraviolet photoelectron spectroscopy (UPS, He I = 21.2 eV, He II = 40.8 eV) were carried out in a Leybold LHS 12 MCD system equipped with an EA 200 analyser. The base pressure of the apparatus was 2×10^{-10} Torr. The energy scale was calibrated

using Au $4f_{7/2} = 84.0$ eV. The quantitative results were obtained after Shirley background substraction and integration using empirically derived cross sections of [25]. The $CoTe_x$ samples were transferred into the preparation chamber (base pressure 1×10^{-9} mbar) as loose powders in a mortar-like stainless steel sample holder. A wobble stick (VG Instruments) equipped with a stainless steel pestle was used to grind the samples in UHV.

Table 2. Atomic coordinates, equivalent displacement parameter U_{eq} (Å^2) and anisotropic displacement parameters for $CoTe_2$ and $CoTe_{1.3}$. Note: the Co2 atom in $CoTe_{1.3}$ was refined with an isotropic displacement parameter.

$CoTe_2$	x	y	z	U_{eq}		
Co	0	0	0	0.0079(1)		
Te	0.220 76(4)	0.363 60(3)	0	0.007 11(8)		
	U_{11}	U_{22}	U_{33}	U_{23}	U_{13}	U_{12}
Co	0.007 52(27)	0.007 93(30)	0.008 34(32)	0	0	−0.000 15(20)
Te	0.006 57(15)	0.006 91(14)	0.007 85(14)	0	0	0.000 67(6)
$CoTe_{1.3}$	x	y	z	U_{eq}		
Co1	0	0	0	0.0088(5)		
Co2	0	0	0.5	0.0097(8)		
Te	2/3	1/3	0.2461(2)	0.0074(3)		
	U_{11}	U_{22}	U_{33}	U_{23}	U_{13}	U_{12}
Co1	0.0098(6)	0.0098(6)	0.0068(9)	0	0	0.0049(3)
Te	0.0072(4)	0.0072(4)	0.0078(4)	0	0	0.0036(2)

The band structure of stoichiometric $CoTe_2$ with the CdI_2- and marcasite-type structures have been calculated charge self-consistently by means of the linear muffin tin orbital (LMTO) method [26] in the ASA mode. Exchange and correlation have been treated within the framework of local density functional theory using the parametrization of Hedin and Lundqvist. Relativistic effects have been accounted for by using the so-called scalar-relativistic approximation ignoring the influence of spin–orbit coupling. For the basis functions a maximum angular momentum of $l_{max} = 2$ has been used for all components. The results presented here have been obtained by using the tetrahedron method performing the necessary Brillouin zone (BZ) integration with 840 and 864 k points during the SCF cycles. Important numerical results are listed in table 4.

3. Results and discussion

3.1. The crystal structures

The x-ray powder patterns of $CoTe_x$ samples with $x = 1.3$–1.7 could be indexed on the basis of the trigonal CdI_2-type structure. The lattice parameters are $a = 3.893(1)$ Å, $c = 5.371(1)$ Å ($c/a = 1.380$), $a = 3.8223(4)$ Å, $c = 5.388(1)$ Å ($c/a = 1.410$) and $a = 3.820(1)$ Å and $c = 5.391(4)$ Å ($c/a = 1.411$) for $CoTe_{1.3}$, $CoTe_{1.6}$ and $CoTe_{1.7}$, respectively, which agree well with the data reported in the literature. For samples with $1.7 \leqslant x \leqslant 2$ the CdI_2- and marcasite-type structures coexist. This finding is in agreement with the observations reported earlier [7, 11, 16].

Table 3. Interatomic distances (Å) for $CoTe_2$ and $CoTe_{1.3}$. The super- and subscripts refer to the definitions provided in the diagrams in the the lower part of the table for $CoTe_2$ (marcasite) (left) and $CoTe_{1.3}$ (CdI_2 type) (right).

$CoTe_2$			
Te–Te^a	2.916(1)	Te–Te^b	3.439(1)
Te–Te^c	3.601(1)	Te–Te^c	3.729(1)
Co–Te 2×	2.582(1)	Co–Te 4×	2.602(1)
$CoTe_{1.3}$			
Co(1)–Te 6x	2.608(1)	Co(1)–Co(2)	2.686(1)
Co(2)–Te 6x	2.629(1)		
Te–Te$_{intra}$	3.470(1)	Te–Te$_{inter}$	3.534(1)
Te–Te$_{\parallel\ layer}$	3.893(1)		

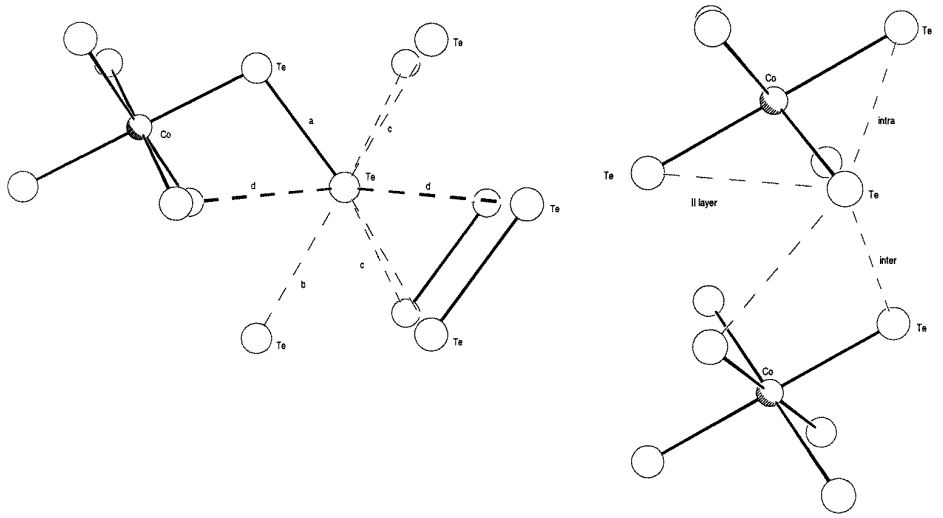

For $CoTe_2$ with the orthorhombic marcasite-type structure the two space groups $Pnn2$ or $Pnnm$ are possible. The first crystal structure determination was performed in the centrosymmetric space group $Pnnm$ [14]. Later, a detailed study of the anisotropic displacement parameters of Co and Te led to the conclusion that $CoTe_2$ adopts the acentric space group $Pnn2$ [10]. A further study of the prototype FeS_2 (marcasite) [27] revealed that the deviation of the z parameter of S from zero was within the estimated standard deviation giving no evidence for the absence of the mirror plane. Furthermore a recent investigation of iron ditelluride $FeTe_2$ (marcasite) shows that it crystallizes in the centrosymmetric space group $Pnnm$ [28]. It was argued that absorption effects were responsible for the uncertainties in the earlier studies of the crystal structure of $CoTe_2$.

In the present work the refinement of the crystal structure of $CoTe_2$ was performed in both space groups. The refinement in $Pnn2$ revealed that the z parameter of Co is zero within three times the standard deviation ($-0.000\,88(116)$). In addition the analysis of the anisotropic displacement factors give no hints of the absence of the mirror plane. Hence, the final refinements were performed in the centrosymmetric space group $Pnnm$.

The structure of $CoTe_2$ is build up by pairs of Te_2 ions lying in the ab plane. They are arranged alternatingly diagonally within the unit cell [8, 10]. The Co atoms are in a nearly

Table 4. Numerical results of band structure calculations for CdI_2-type and marcasite-type $CoTe_2$. S(atom) is the Wigner–Seitz radius in multiples of the Bohr atomic radius; Q(atom) is the charge transfer; the contributions of the different atoms to the DOS at E_F and the total DOS are given in states eV^{-1}/atom/spin. Note: the lattice parameters for $CoTe_2$ were taken from [16].

	$CoTe_2$ (CdI_2)	$CoTe_2$ (marcasite)
a [Å]	3.802	5.3267
b [Å]		6.3219
c [Å]	5.4094	3.9059
Co DOS	0.841	1.867
Co s DOS	0.008	0.037
Co p DOS	0.190	0.075
Co d DOS	0.643	1.755
Te DOS	0.476	0.457
Te s DOS	0.012	0.079
Te p DOS	0.398	0.308
Te d DOS	0.067	0.071
Total	1.793	2.781
Q (Co)	0.04	0.014
Q(Te)	−0.02	−0.007
S(Co)	2.760	2.760
S(Te)	3.531	3.489
k points	840	864

perfect octahedral environment of Te centres. The $CoTe_6$ octahedra share common edges parallel to the c axis and have common corners within the ab plane (see figure 1).

The Te–Te distance in the Te_2 pair amounts to 2.916(1) Å, longer than the Te–Te distance in elemental Te (2.76 Å) or in Te_2^{2-} containing phases like $HfTe_5$ [45] or $ZrTe_3$ [46], but in the range which is treated as a weaken single bond. The shortest distance between the

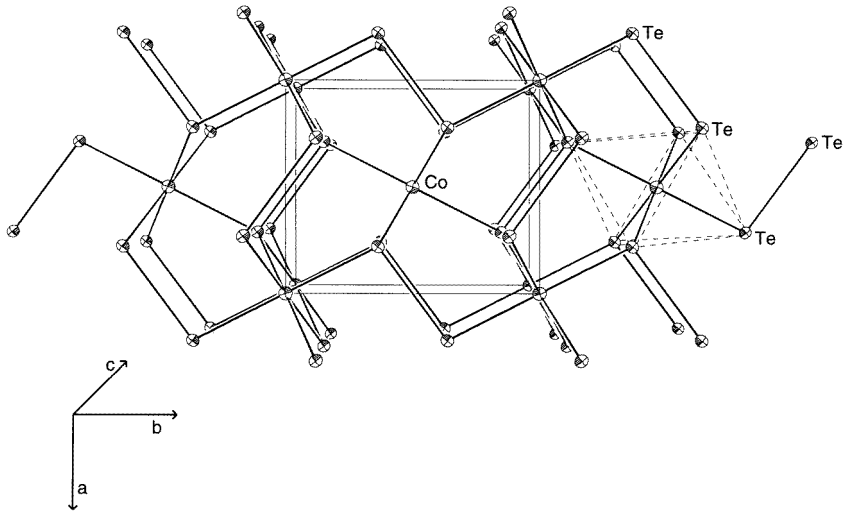

Figure 1. The crystal structure of marcasite-type $CoTe_2$. One $CoTe_6$ octahedron is outlined with the dotted lines.

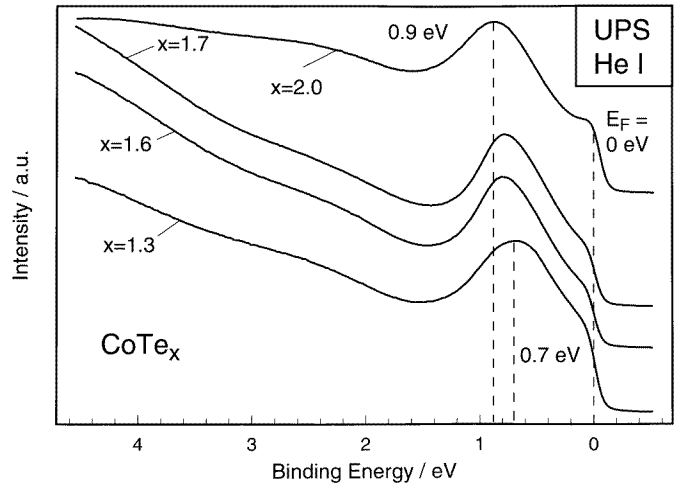

(a)

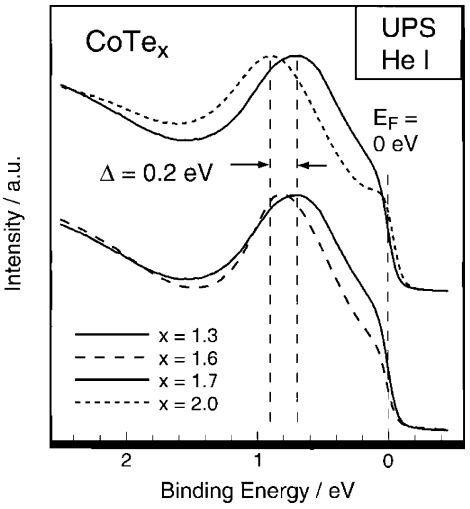

(b)

Figure 2. (a) The He I valence band region of the $CoTe_x$ samples ($x = 1.3$, 1.6, 1.7 and 2.0). (b) Enlarged view of the He I valence band region of the $CoTe_x$ samples ($x = 1.3$, 1.6, 1.7 and 2.0) around the Fermi energy.

pairs is 3.439 Å, clearly longer than within the pairs but about 0.7 Å shorter than the sum of the ionic radii of Te^{2-} anions. In addition, every Te has four Te neighbours at 3.601 Å and four additional Te at 3.729 Å, leading to a complex polymeric Te–Te network (see the sketch in table 3). Averaging all Te–Te distances below about 3.6 Å the ⟨Te–Te⟩ amounts to 3.46 Å.

The refinement of the crystal structure of a single crystal with nominal composition $CoTe_{1.3}$ was started assuming the CdI_2 structure type with Co1 on site 1a and Co2 on site 1b located in the van der Waals gaps. The refinement clearly showed that the crystal was twinned with the twin plane 001. The subsequent refinements resulted in a twin fraction of 27(1)%. With a fixed displacement factor for Co2 comparable to the U_{eq} of Co1 the site

occupation factor converged to 0.050(2) resulting in a final R value of 2.13%, and a final composition of this crystal of $CoTe_{1.25(2)}$. The c/a ratio of 1.380 is in good agreement with values reported in the literature for a composition near $CoTe_{1.3}$ [7, 11, 16]. The Co1 centres in the full layers have Co2 neighbours at about 2.69 Å, which is only 0.19 Å longer than in Co metal. The shortest Te–Te intralayer contact amounts to 3.470 Å and the interlayer distance is 3.534 Å, with an average of 3.502 Å and clearly shorter than the sum of two Te^{2-} ionic radii. We note that this value is only 0.042 Å longer than the average obtained for marcasite $CoTe_2$. Using the axes of the $CoTe_{1.7}$ sample an average Te–Te distance of 3.482 Å is calculated, a shortening of the interatomic Te–Te separation by about 0.02 Å. These relatively short distances suggest Te–Te bonding and the low c/a ratio is easily understood.

The intralayer distance is identical to that found in $NiTe_2$ [6], but the interlayer contact is longer in agreement with the different c/a ratios of the two tellurides ($Ni_{1.027(5)}Te_2$: 1.365; $CoTe_{1.3}$: 1.380). In marcasite $CoTe_2$ the Co–Te distances range from 2.582(1) Å to 2.602(1) Å with an average ⟨Co–Te⟩ of 2.594 Å. Assuming a radius of 2.11 Å for Te^{2-} the radius for Co is about 0.484 Å, clearly smaller than the values tabulated in the literature for Co^{2+}($r(Co^{2+}) = 0.65$ Å, low spin) [47]. The calculation of the expected Co–Te distance using the oxide radius of Co^{2+} yields 2.76 Å. If we subtract this value from the observed average Co–Te distance a negative value of -0.166 Å is obtained. It is generally accepted that M–Te bonds are more covalent than M–O bonds and hence the contraction of the telluride distance relative to the oxide distance can be attributed to the covalence occurring in our system due to the smaller electronegativity difference between Co and Te. On the other hand, if the oxide radius for Co^{2+} is used, we calculate $r(Te^{2-}) = 1.944$ Å.

In $CoTe_{1.3}$ the Co1–Te and Co2–Te distances of 2.609 Å and 2.632 Å are longer than in the marcasite sample, and they are reduced to about 2.576 Å and 2.596 Å for $CoTe_{1.7}$ (calculated using the lattice parameters of $CoTe_{1.7}$). The decreasing Co–Te distances with increasing Te content suggest a change of the valence state of the Co centres, in agreement with the decrease of d-electron density located on the Co when the Te content is raised.

To the best of our knowledge no other Co tellurides with Co atoms in an octahedral environment are reported in the literature. In the ternary tellurides $Nb_2Co_2Te_4$, $TaCo_2Te_2$ [48], $NbCoTe_2$ [49, 50], $TaCoTe_2$ [50] the Co atoms are either in a tetrahedral coordination or threefold coordinated by Te. The Co–Te distances in these compounds scatter between 2.479 Å and 2.649 Å and the average is about 2.56 Å.

3.2. The electronic structure

3.2.1. The experimental electronic structure. The valence band spectra of $CoTe_x$ ($x = 1.3$, 1.6, 1.7 and 2) recorded with He I and He II are displayed in figures 2(a), 2(b) and 3, respectively. The heights of the emission intensity at the emission threshold convincingly reveal that all samples are metals. With both excitation energies the density of states at E_F decreases with increasing Te content for samples with the CdI_2-type structure. These changes are associated with the decrease of the intensity of a not well resolved peak directly located below E_F. This can be seen more clearly in figure 2(b) which shows an enlarged view of the region around the Fermi energy. In $CoTe_2$ the Fermi level cuts this peak near the emission maximum. A well resolved peak is located below E_F which shifts from 0.7 eV to 0.9 eV when going from $CoTe_{1.3}$ to $CoTe_2$.

The differences between the He I and He II spectra are due to the different cross sections for the excitation energies of He I and He II, and using the cross sections for the different excitation energies given by Yeh and Lindau [29] (He I: Te 5p, 4.758; Co 3d, 4.356. He II:

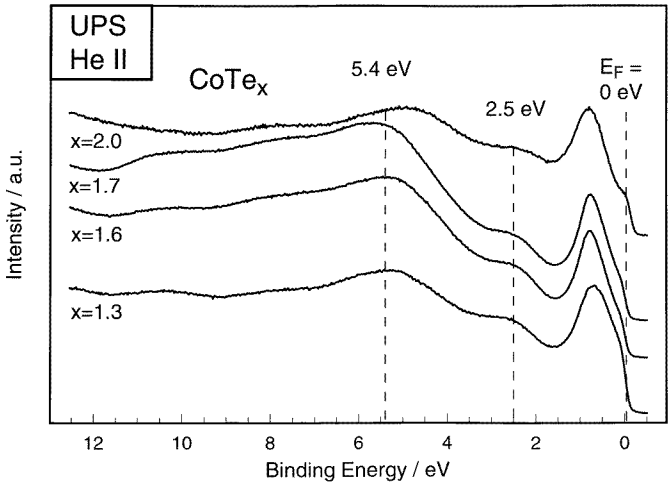

Figure 3. The He II valence band region of the $CoTe_x$ samples ($x = 1.3$, 1.6, 1.7 and 2.0).

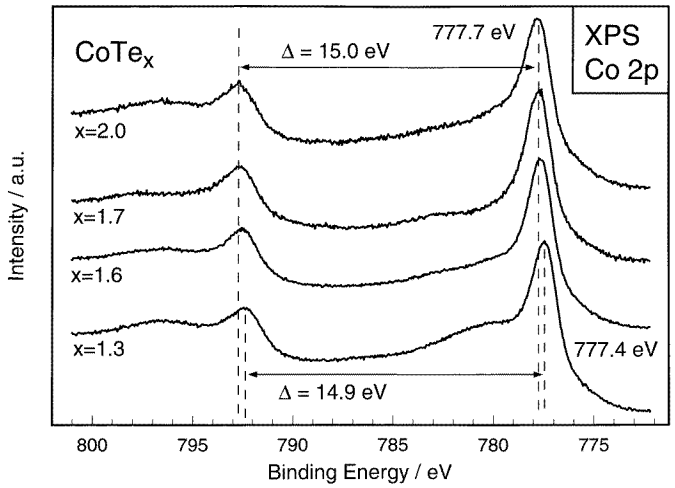

Figure 4. The Co 2p core level region of the $CoTe_x$ samples ($x = 1.3$, 1.6, 1.7 and 2.0).

Te 5p, 0.5043; Co 3d, 8.738) a qualitative assignment of the different emissions seems to be possible. The height of the emission at the Fermi level is slightly lower for He II than for He I. If only Co 3d contributes to the DOS at E_F, the height should be twice as large in the He II spectra. On the other hand, if only Te 5p states are responsible for the DOS at E_F, the emission should be about nine times smaller in the He II spectra. Hence, it can be assumed that both Co 3d and Te 5p states contribute to the DOS at E_F.

For He I the cross sections for Co 3d and Te 5p are comparable. Therefore, if the emission at E_F is due to Co 3d as well as Te 5p states in the proportions of composition it should increase from $x = 1.3$ to $x = 1.7$ by about 10%, in contrast to what is observed. In addition, a rough estimate shows that the expected height of the DOS for $CoTe_2$ should be about 20% larger than for $CoTe_{1.3}$. This value is clearly smaller than the value estimated from the spectra (30%).

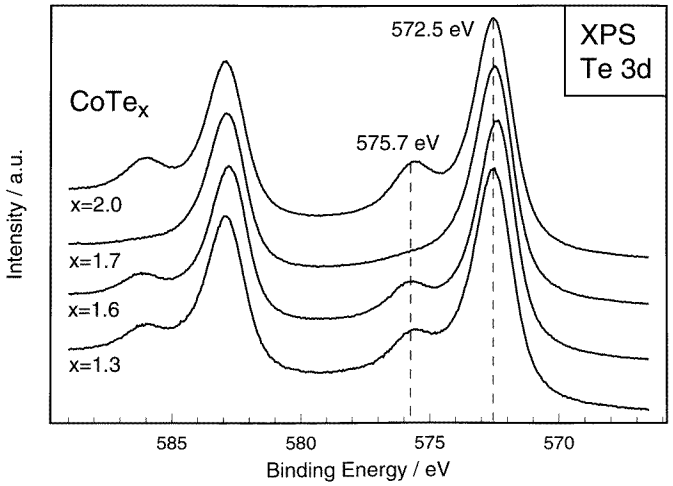

Figure 5. The Te 3d core level region of the $CoTe_x$ samples ($x = 1.3$, 1.6, 1.7 and 2.0). Note: the small peak at 575.7 eV is caused by a tellurium oxide on the surface of the samples.

A similar discussion can be given for the changes in the He II spectra. The cross section for Co 3d for this radiation is about 17 times larger than for Te 5p. Consequently, if the emission at E_F is only caused by the increased contributions of Te 5p states an increase of the DOS at the Fermi level of about 1% is expected when x is raised from 1.3 to 1.7, and this increase should only amount about 3% between $CoTe_{1.3}$ and $CoTe_2$. Such small changes are outside the limits of the method and contradict the observations in the He II spectra.

The detailed analysis of the spectra in connection with alterations of the cross sections as function of radiation let us conclude that Te 5p and Co 3d states both contribute to the emission at E_F, but the changes observed are mainly due to the change of contributions of Co 3d states. This implies that the 3d electron density is reduced when x is increased from 1.3 to 1.7. This conclusions are in accordance with general considerations. In $CoTe_{1.3}$ the Co centres have the formal oxidation state $+2.6$ ($3d^{6.4}$), which increases to $+3.4$ for $CoTe_{1.7}$, i.e. a decrease of the Co 3d electron density.

The peak at about 0.7–0.9 eV below the Fermi level is mainly due to Co 3d states. The shift by 0.2 eV to higher binding energies for $CoTe_2$ is probably due to the different electronic band structure. In $CoTe_2$ there are Te_2^{2-} anions and Co is in the formal oxidation state $+2$ ($3d^7$).

Two additional emissions are observed in the He II spectra located at about 2.5 and 5.4 eV below E_F (figure 3). These peaks are caused by Te p states which are hybridized with Co d states.

The Co 2p core level region for the $CoTe_x$ ($x = 1.3$, 1.6, 1.7, 2.0) samples are displayed in figure 4. The intense peaks centred at 777.4 and 777.7 eV, respectively, are due to the Co $2p_{3/2}$ core level, and the Co $2p_{1/2}$–$2p_{3/2}$ spin–orbit coupling amounts to about 15 eV. The full width at half maximum (FWHM) is 1.8(1) eV for $x = 1.3$, 1.6 and 1.7 and slightly increases to 2.1(1) eV for $CoTe_2$. We note that the FWHM is nearly identical to the value given for metallic Co and it is significantly smaller than the value reported for CoO ($\approx$3.6 eV). The slightly broader peak for $CoTe_2$ may be caused by unresolved final-state effects.

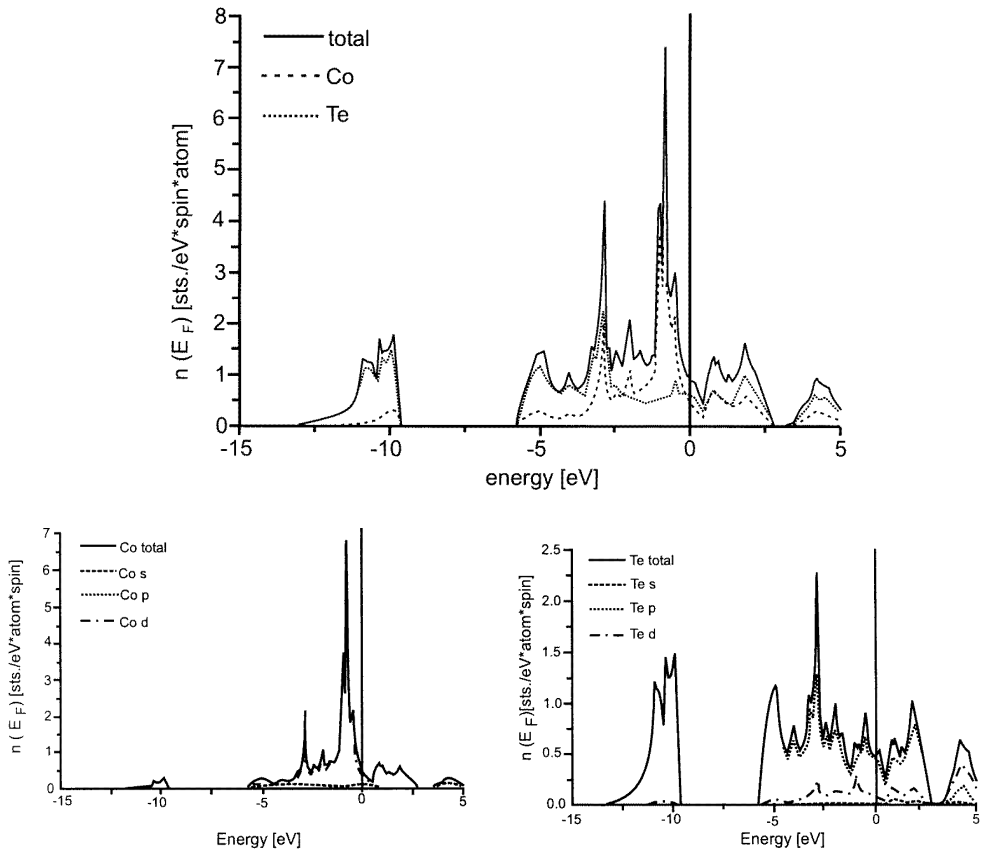

Figure 6. The calculated density of states curve for $CoTe_2$ with the CdI_2-type structure (top). Bottom: the contributions of Co (left) and of Te (right).

The binding energy of the Co $2p_{3/2}$ core level shifts from 777.4 eV to 777.7 eV when the Te content is raised from $x = 1.3$ to $x = 1.7$ indicative of a reduced electron density located on the Co centres, in good agreement with what is expected from formal considerations. But for the stoichiometric sample the binding energy of 777.7 eV is identical to that obtained for $CoTe_{1.7}$. This observation can only be explained on the basis of different Madelung contributions to the chemical shifts. As discussed above in the $CoTe_x$ phases with the CdI_2 structure the Co centres in the full metal atom layers have short contacts to the Co centres in the van der Waals gaps. With increasing Te content the number of Co–Co contacts is reduced and in $CoTe_{1.7}$ only 30% of the Co atoms in the full layers have Co neighbours in the van der Waals gaps. The next-nearest Co neighbours are located within the full layers at the distance of the a axis, which amounts to 3.821 Å in $CoTe_{1.7}$, a value comparable to the shortest Co–Co distance in $CoTe_2$ (3.906 Å). Therefore, it is rather a change of the Madelung contribution which causes the small shift of the Co $2p_{3/2}$ core level than a 'true' chemical shift due to alterations of the electron density located on the Co atoms.

The evaluated binding energies for the $2p_{3/2}$ level are in the range of the values reported for elemental Co (NIST XPS database: Co $2p_{3/2}$: 777.8 eV–778.5 eV, average: 778.2 eV). They are lower than the values tabulated for different Co chalcogenides like

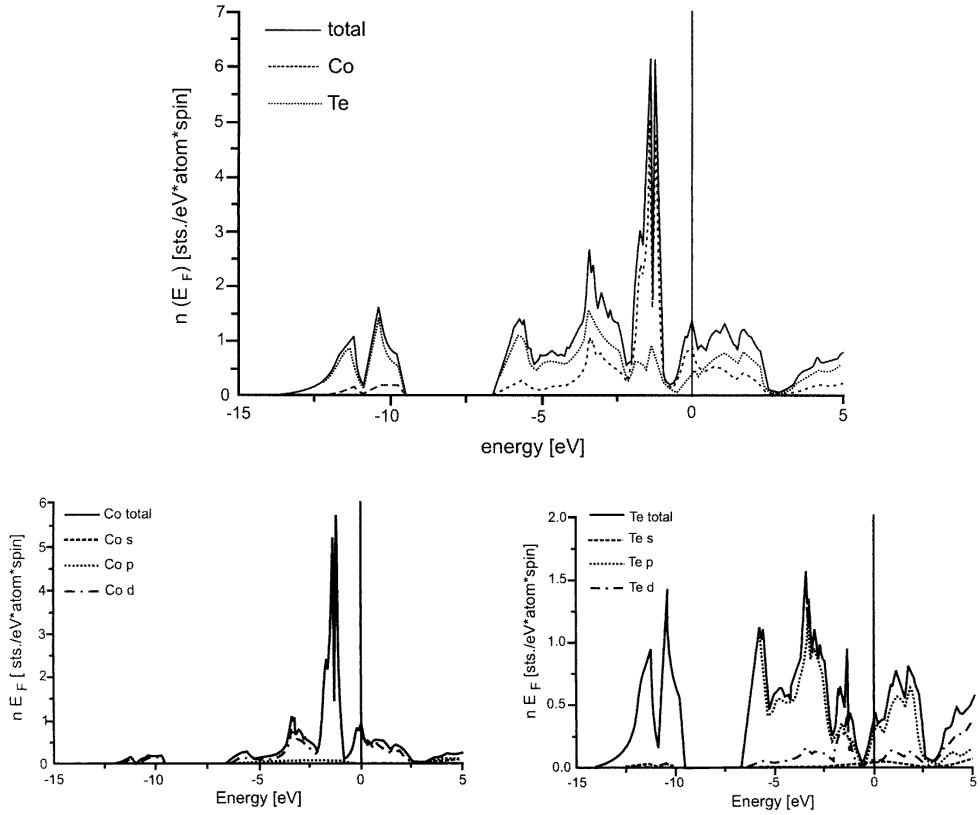

Figure 7. The calculated density of states curve for $CoTe_2$ with the marcasite-type structure (top). Bottom: the contributions of Co (left) and of Te (right).

Co_9S_8 (778.5 eV), $CoMo_2S_4$ (778.9 eV) [30], CoS_2 (778.1 eV) or $CoSe_2$ (778.3 eV) [31] or CoSe (778.7 eV) [32] and Co oxides (780–781.3 eV). But they are significantly lower than the binding energies given for Co(II) halides (780.5–783 eV) or more ionic Co(II) compounds (782.4–782.6 eV) [33].

The small emission at about 780.4 eV is caused by a slight surface contamination by CoO. From the ratios of the peak areas of the main peak and of the oxide peak we estimated that the contamination is less than 5%.

The not well pronounced structures above about 781.5 eV are due to shake-up satellite structures, as observed in CoF_2, $CoCl_2$ [34], $Co(acac)_2$ [35] or CoO. The energy separation between the main peak and the shake-up satellite depends on the covalency of the Co-X bonds. For CoO it amounts to about 9.6 eV. Because the shake-up satellites are not well resolved, the energy separation between the main peak and the satellites is difficult to determine. But a rough estimate yields about 4.5 eV, an energy separation reflecting the pronounced covalency of the Co–Te bond.

The Co $2p_{3/2}$ peaks exhibit an asymmetric shape towards the high-binding-energy side. Such an asymmetry was reported for metallic CoS_2 (pyrite type) and was attributed to the coupling of the core hole with the conduction electrons [36]. Because all $CoTe_x$ samples are metals with a high DOS at the Fermi level the observed asymmetry may also be caused by such a coupling process.

The Te 3d core level region is displayed in figure 5. The evaluated binding energy of the Te $3d_{5/2}$ core level of 572.5 eV is smaller than the values given for elemental Te (572.98 and 572.85 eV [37, 38]; average: 572.9 eV using 18 data; range: 572.1 to 573.54 eV), but it is significantly lower than in Te halides or oxides (575.8–576.9 eV [39, 40]). Compared with the binding energy published for the ditellurides $IrTe_2$ or Ir_3Te_8 (573.0 eV and 573.5 eV [1]) and $NbTe_4$ (572.8 eV [41]), the values obtained for the $CoTe_x$ samples are lower and can better be compared with the binding energies reported for monotellurides (ZrSiTe: 572.5 eV [42]; CdTe: 572.47 eV [43]), $Nb_3Te_{4-y}As_y$ (572.4 eV [51]) or $NiTe_2$ (572.3 eV [6]). The estimated FWHM is identical for all $CoTe_x$ samples and amounts to 1.8(1) eV, indicative for only one Te species in all $CoTe_x$ samples. The small peak at about 575.5 eV is caused by a slight surface contamination by TeO_2.

In general, the binding energies listed in the NIST XPS database for the different tellurium compounds scatter by about ± 0.5 eV for the same compound. A rough estimate of the binding energies versus oxidation state yields a chemical shift of the Te $3d_{5/2}$ core level line of about 0.6 eV per oxidation number. The average binding energy of the $3d_{5/2}$ emission for elemental Te is found to be 572.9 eV. Hence, a shift of 0.4 eV relative to elemental Te and assuming a linear relationship between chemical shift and oxidation number would lead to an oxidation number for Te < -1 in all $CoTe_x$ samples. Using the relation between the Te–Te distances versus oxidation states given in [1] an oxidation state of about -1.3 for the Te in $CoTe_2$ would be deduced.

The Te 3d peaks for all samples exhibit a pronounced tail on the high-binding-energy side. Such highly asymmetric core level lines are observed for the Cu 2p core level as well as for the S 2p peaks of binary Cu sulphides and selenides [36, 44], which are metals. This asymmetry was attributed to the coupling of the core hole with the delocalized electron density located near the Fermi level. Because the Co tellurides are metals and Te states contribute significantly to the density of states at the Fermi level this final-state effect may be the reason for the asymmetric line shape of the Te 3d core levels.

3.2.2. The theoretical electronic band structures. The calculated total density of states curves (DOS) for $CoTe_2$ with the CdI_2- and marcasite-type structure are displayed in figures 6 and 7, respectively. The most important numerical results and lattice parameters are summarized in table 4. As figures 6 and 7 show, the Te 5s states give rise to a narrow band at a binding energy of 9.5–14 eV with only weak hybridization with Co states. In the marcasite type the Te 5s band is clearly split into two subbands separated by a minimum.

The lower part of the valence band (VB) (-5.8 eV to -1.5 eV for CdI_2 type and -6.6 eV to -2.2 eV for marcasite type) is dominated by Te p states. This lower part of the VB is separated by a DOS minimum from a narrow peak centred at about -0.8 eV for CdI_2 and at about -1.2 eV for marcasite type. These sharp peaks are dominated by Co 3d states. For the CdI_2 modification the DOS sharply decreases above the peak, giving rise to a value of 1.793 states eV^{-1}/FU at the Fermi level (FU = formula unit). For the marcasite-type structure a pronounced minimum in the DOS curve is observed at about -0.6 eV. Above this dip the DOS increases again, yielding a value of 2.781 states eV^{-1}/FU at E_F.

As can be seen from the figures and from table 4 the contributions from Te states to the DOS is about 50% in the CdI_2-type and about 35% in the marcasite-type structure. The Te d states contribute about 15% to the total Te contributions. This behaviour cannot be understood on the basis of a simple tight-binding description, ignoring d-valence states of Te.

The crystal field should lead to a splitting of the Co 3d states into t_{2g} and e_g sublevels.

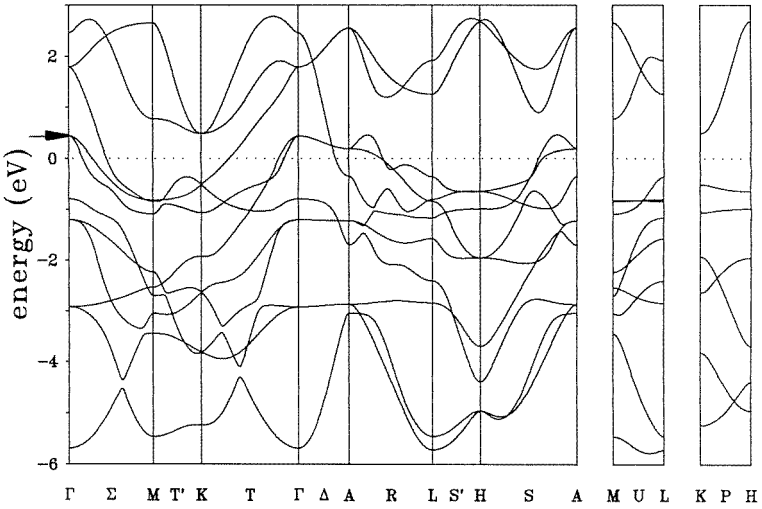

Figure 8. The dispersion relation $E(k)$ for $CoTe_2$ with the CdI_2-type structure.

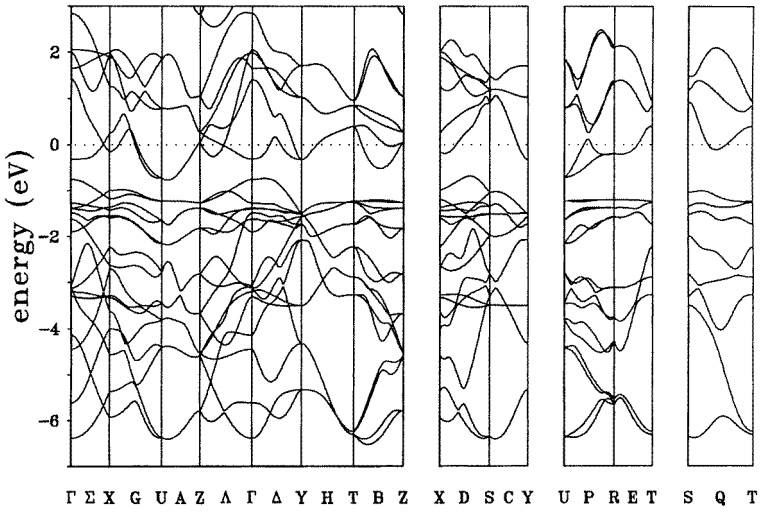

Figure 9. The dispersion relation $E(k)$ for $CoTe_2$ with the marcasite-type structure.

This splitting is seen in the DOS curves (figures 6 and 7). Applying the tight-binding model the change of the oxidation state of Te from -2 in the CdI_2-type samples to -1 in the marcasite-type $CoTe_2$ leads to the occupation of Co 3d states which are empty in the CdI_2 samples, and shifts the Fermi energy to higher energies. This can nicely be seen comparing the DOS curves for $CoTe_2$ (CdI_2) and $CoTe_2$ (marcasite). For the latter the Fermi energy cuts the peak which is located above E_F in the former compound.

The numerical results obtained for $CoTe_2$ in the two modifications must be compared with some care. For the calculations of the electronic band structure of the CdI_2 type an ideal stoichiometry $CoTe_2$ was assumed. As was discussed above this structure type is only stable up to a composition $CoTe_{1.7}$. That means that due to the higher occupancy of

the Co 3d states the Fermi level cuts the DOS curve at slightly higher energies leading to a lower DOS at E_F in reality than those calculated. It was reported that the electrical conductivity of $CoTe_x$ samples decreases with increasing Co content [12, 19], in agreement with the above-presented considerations.

It must be noted here that the interpretations of the experimental valence band spectra given above are in full agreement with the calculated density of states curves.

A rather detailed insight into the anisotropy of the chemical bonding is supplied by the dispersion relations $E(k)$ shown in figures 8 and 9. For the CdI_2-type structure the Fermi level crosses at least 3 conduction bands in the directions Γ–M and Γ–K, both in the basal plane of the structure (figure 8). These bands exhibit in part a large dispersion indicating strong bonding interactions between the atoms in that plane. We note that in the direction Γ–A perpendicular to the basal plane one conduction band also crosses the Fermi level, showing a rather large dispersion. In the other two directions (M–L, K–H) the highest conduction bands are well below E_F. Another interesting feature of the $E(k)$ relation is the observation of band crossing points near the Fermi level in the directions A–L and H–A. As mentioned above, the calculations were done with the assumption of stoichiometric $CoTe_2$ using the lattice parameters given for $CoTe_2$. Within the framework of the rigid-band model the insertion of excess Co in the van der Waals gaps of the structure should lift the Fermi level (see the arrow in figure 8) removing this unfavourable situation, and the resulting dispersion relation becomes very similar to that of stoichiometric $NiTe_2$ [6].

For marcasite-type $CoTe_2$ the dispersion relation clearly demonstrates the three-dimensional character of the material (figure 9). In all directions of the BZ at least the highest conduction band crosses the Fermi level.

Acknowledgments

The authors would like to thank Professor H Ebert and M Knecht for their technical support and encouraging discussions.

References

[1] Jobic S, Brec R and Rouxel J 1992 *J. Solid State Chem.* **96** 169
[2] Monconduit L, Evain M, Boucher F, Brec R and Rouxel J 1992 *Z. Anorg. (Allg.) Chem.* **616** 177
[3] Jobic S, Evain M, Brec R, Deniard P, Jouanneaux A and Rouxel J 1991 *J. Solid State Chem.* **95** 319
[4] Canadell E, Jobic S, Brec R and Rouxel J 1992 *J. Solid State Chem.* **98** 59
[5] Canadell E, Jobic S, Brec R, Rouxel J and Whangbo M H 1992 *J. Solid State Chem.* **99** 189
[6] Bensch W, Heid W, Muhler M, Jobic S, Brec R and Rouxel J 1996 *J. Solid State Chem.* **121** 87
[7] Schicketanz H, Terzieff P and Komarek K L 1986 *J. Less-common Met.* **119** 13
[8] Tengner S 1938 *Z. Anorg. (Allg.) Chem.* **239** 126
[9] Chetal A R, Mahto P and Sarode P R 1988 *J. Phys. Chem. Solids.* **49** 279
[10] Brostigen G and Kjekshus A 1970 *Acta Chem. Scand.* **24** 1925
[11] Klepp K O and Komarek K L 1973 *Monatsh. Chem.* **104** 105
[12] Dudkin L D and Dyul'dina K A 1959 *Russ. J. Inorg. Chem.* **4** 1056
[13] Binczycka H, Hafner S S, Moh G and Stanek J 1990 *Phys. Lett.* **145A** 467
[14] Buerger M J 1931 *Am. Mineral.* **16** 361
[15] Gibart P and Vecherant C 1969 *J. Cryst. Growth* **5** 111
[16] Haraldsen H, Gronvold F and Hurlen T 1956 *Z. Anorg. (Allg.) Chem.* **283** 143
[17] Ehrlich P 1949 *Z. Anorg. Chem.* **260** 19
[18] Hulliger F 1968 *Structure Bonding* **4** 89
[19] Saut G 1965 *C. R. Acad. Sci., Paris* **261** 3339
[20] Dallacasa V and Ortalli I 1980 *J. Phys. C: Solid State Phys.* **13** 2055
[21] Fano V and Ortalli I 1971 *J. Phys. Chem. Solids* **32** 2305

[22] Vandenbempt E, Pauwels L and de Clippeleir K 1971 *Bull. Soc. Chim. Belges* **80** 283
[23] Stanek J, Khasanov A M and Hafner S S 1992 *Phys. Rev.* B **45** 56
[24] Terzieff P 1984 *Solid State Commun.* **50** 151
[25] Briggs D and Seah M P 1990 *Practical Surface Analysis* 2nd edn, vol 1 (New York: Wiley)
[26] Skriver H L 1983 *The LMTO Method* (Berlin: Springer)
[27] Brostigen G, Kjekshus A and Romming Chr 1973 *Acta Chem. Scand.* **27** 2791
[28] Pertlik F 1986 *Anz. Österr. Akad. Wiss., Math. Naturwiss. Kl.* **123** 123
[29] Yeh J J and Lindau I 1985 *At. Data Nucl. Data Tables* **32** 1
[30] Candia R, Clausen B S and Topsoe H 1982 *J. Catal.* **77** 397
[31] van der Heide H, Hemmel R, van Bruggen C F and Haas C 1980 *J. Solid State Chem.* **33** 17
[32] Mandale A B, Badrinarayarian S, Date S K and Sinha A P B 1984 *J. Electron. Spectrosc. Relat. Phenom.* **33** 61
[33] Hernan L, Morales J, Sanchez L, Tirado J L, Espinos J P and Elipe A R G 1995 *Chem. Mater.* **7** 1576
[34] Wallbank B, Main I G and Johnson C E 1974 *J. Electron. Spectrosc. Relat. Phenom.* **5** 259
[35] Carlson T A, Carver J C, Saethre L J, Santibanez F G and Vernon G A 1974 *J. Electron. Spectrosc. Relat. Phenom.* **5** 247
[36] Folmer J C W and DeBoer D K G 1981 *Solid State Commun.* **38** 1135
[37] Nyholm R and Martensson N 1980 *J. Phys. C: Solid State Phys.* **13** L279
[38] Laine E, Tamminen M, Makela R and Pessa M 1983 *J. Mater. Sci.* **18** 295
[39] Bahl M K, Watson R L and Irgolic K J 1977 *J. Phys. Chem.* **66** 5526
[40] Ricco A J, White H S and Wrighton M S 1984 *J. Vac. Sci. Technol.* A **2** 910
[41] Bahl M K 1975 *J. Phys. Chem. Solids* **36** 485
[42] Muhler M, Bensch W, Helmer O, Knecht M and Ebert H 1994 *J. Phys. Chem.* **99** 3326
[43] White H S, Ricco A J and Wrighton M S 1983 *J. Phys. Chem.* **87** 5140
[44] Folmer J C W and Jellinek F 1980 *J. Less-common Met.* **76** 153
[45] Furuseth S, Brattas L and Kjekshus A 1973 *Acta Chem. Scand.* **27** 2367
[46] Furuseth S and Fjellvag H 1991 *Acta Chem. Scand.* **45** 694
[47] Shannon R D 1976 *Acta Crystallogr.* A **32** 751
[48] Tremel W 1991 *J. Chem. Soc. Chem. Commun.* 1405
[49] Li J, Badding M E and DiSalvo F J 1992 *Inorg. Chem.* **31** 1050
[50] Li J, McCulley F, McDonnell S L, Masciocchi M, Proserpio D M and Sironi A 1993 *Inorg. Chem.* **32** 4829
[51] Bensch W, M.Schnieder, Muhler M, W.Biberacher, Knecht M, Vernes A and Ebert H 1996 *J. Alloys Compound* **244** 59